8th International Conference
on
Wind Turbine Noise
Lisbon – 12th to 14th June 2019

Numerical study of aerodynamic radiated noise of a Coflow-Jet Vertical Axis Wind Turbine

Dan Radulescu INCDT-COMOTI: dan.radulescu@comoti.ro
Marius Deaconu INCDT-COMOTI: marius.deaconu@comoti.ro
Georgel Vizitiu INCDT-COMOTI: georgel.vizitiu@comoti.ro
Narcisa Burtea INCDT-COMOTI: narcisa.burtea@comoti.ro

Summary

Vertical Axis Wind Turbines (VAWT) represent a suitable solution for urban areas since they are insensitive to wind direction and they produce less noise. One of the shortcomings of VAWT is represented by a lower efficiency comparing with Horizontal Axis Wind Turbine (HAWT). Coflow-Jet (CFJ) represents a new method to improve the aerodynamic performance of the airfoils due to increased circulation on the suction side. Using the CFJ improves the VAWT performance but a noise evaluation should be considered in this case. Operating wind turbines generate tonal and broadband noises affecting the living environment adversely; especially small wind turbines located in the vicinity of human living places. Therefore, it is important to determine the level of noise pollution of such type of wind turbine installation. The current study carries out numerical prediction for aerodynamic noise radiated from an H-Darrieus Vertical Axis Wind Turbine which uses CFJ. Incompressible transient simulation is conducted to obtain the instantaneous turbulent flow field. Noise prediction was performed by the Ffowcs Williams and Hawkings (FW–H) acoustic analogy formulation. Simulations were performed for three different tip-speed ratios (TSR). First, the mean torque coefficient is compared with the basic VAWT which does not use CFJ. Then, the study focuses on the broadband noises of the turbulent boundary layers and the tonal noises due to blade passing frequency. Results indicate a direct relation between the strength of the radiated noise and the rotational speed. Furthermore, noise directivity is investigated. It is concluded that the OASPL (Overall sound pressure level) is strongly reduced both tonal and broadband by the use of CFJ for a VAWT and further optimisation is possible.

1. Introduction

There are two principal types of VAWT rotor: lift-type and drag-type. Drag type rotors work by having greater drag on one side of the rotor axis than the other. Drag-type rotors are very simple, but the high drag on the half of the rotor which is travelling upstream limits their efficiency. In addition, the rotors experience a high level of thrust in the wind direction, which limits their maximum size.

Lift-type rotors use aerofoil shaped blades to generate lift, a component of which is in the direction of rotation, thereby producing torque. These rotors do not have the problems of drag-type rotors and have been shown to be able to achieve power coefficients similar to HAWTs [Paraschivoiu, 2002]. Unlike HAWT rotors, the angle of attack experienced by the blades on a VAWT is a function of azimuth, with the peak in angle of attack occurring near the most upstream point of the rotation. The fluctuation of the angle of attack is a function of the tip speed ratio (TSR), which is defined as the ratio of the blade tip speed to the wind speed. At lower TSR the angle of attack can exceed the static stall angle, which has a significant impact on rotor performance due to the occurrence of dynamic stall on the blades.
A second important feature of VAWT performance is the influence of the wake from the upstream blades. As the lift on the blades fluctuates, they shed vorticity, and this is exacerbated by dynamic stall. At the same time the spanwise variation in the pressure distribution results in a strong tip vortex being formed. The vertical wake is then advected through the rotor volume and subsequently interacts with the blades in the downstream half of the rotation, reducing the blade performance in this region. In the field of wind turbine noise, it is necessary to have an appreciation of the concept of noise annoyance.

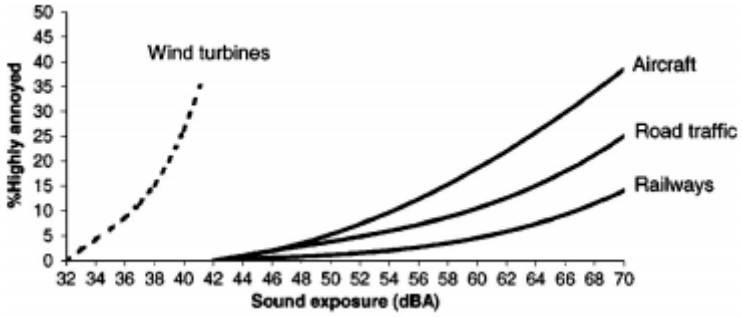

Fig. 1 - Typical annoyance curves

Measurements of wind turbine noise have often indicated that the sound levels radiated by wind turbines are lower than other sources yet still result in greater annoyance (see Figure 1, Pederson and Waye [2004]).

2. Aeroacoustic Noise sources for VAWT

Aeroacoustic noise sources of a VAWT include several categories which produce both tonal and broadband noise. The most important are considered: dynamic stall, blade- wake interaction, incoming turbulence –blade interaction.

2.1 Dynamic stall noise

Both experimental and computational studies have indicated that during dynamic stall an aerofoil can experience significantly unsteady loading. Unsteady forces radiate sound, and the rapid loading fluctuations observed during dynamic stall are likely to be a particularly intense sound source. During operation at lower TSR the blade angles of attack will exceed the static stall angle. Since the blade angle of attack is constantly changing, the blades experience dynamic stall, which results in a significantly different lift and drag behaviour relative to a static aerofoil: Leishman [2006] found that the dynamic loads can exceed the static values by up to 100%. The process of dynamic stall has been found to be dependent on a large number of factors including Mach number, Reynolds number, pitching rate and aerofoil profile, but a general description of the stages of dynamic stall has been outlined by Leishman [2006]. The stages of dynamic stall were first described by Carr et al. [1977] based on data from hot-wire measurements. The sequence below summarises the key points, such that they correspond to the five stages.

1. The aerofoil initially passes the static stall angle without any detectable change in the flow over the aerofoil and the boundary layer remains thin with no evidence of flow reversal. As the

aerofoil incidence increases further, the flow in the boundary layer starts to reverse at the surface.
2. Larger eddies start to form and full flow reversal moves from the trailing-edge to the leading-edge. When the flow reversal reaches the leading-edge, a strong leading-edge vortex is formed.
3. As the angle of attack continues to increase the separated leading-edge vortex grows and advects along the blade chord resulting in a loss of lift at the leading edge and a shift of the centre of pressure to the aft of the blade. This is the cause of the abrupt change in the pitching moment coefficient which is typically described as 'moment stall'. Carr et al. [1977] observed that the peak in the pitching moment curve occurred just before the core of the leading-edge vortex passes over the trailing edge of the blade. It is this large, intense vortex that maintains flow curvature over the aerofoil and prevents lift stall. As the vortex moves towards the trailing edge however, the flow curvature starts to reduce and the lift coefficient starts to drop.
4. Once the leading-edge vortex has passed off the trailing edge the aerofoil can no longer produce the flow curvature required for lift generation, and an abrupt drop in the lift coefficient occurs. After this point the flow over the aerofoil is fully separated as seen in full static stall hence the lift and drag coefficients tend towards their static values. Other smaller vortices may continue to form and be shed from the trailing edge resulting in further unsteadiness in the blade loading.
5. As the blade pitches down the flow attaches from the leading edge. The reattachment point moves along the blade chord at a velocity of approximately 25-35% of the free stream velocity. Depending on the pitching rate the process of reattachment may not be complete until the aerofoil is well below the static stall angle, so the static values of lift and drag will not be achieved until a lower angle of attack. Carr et al. [1977] noted that even once the flow is fully reattached the potential flow does not appear to return to unstalled conditions until the blade has passed its minimum angle and is already on the upstroke.

2.2 Blade wake interaction

The vorticity transport model simulations indicated that there are potentially significant interactions between the wake from the upstream half of the rotor and the downstream blades. In particular, the intense vortices shed from the upstream blade tips are seen to cause strong blade vortex interactions. These interactions with the tip vortices were shown to be more intense at higher TSR [Scheurich, 2011]. Another possible region of blade wake interaction was highlighted by Castelli et al. [2011] who suggested that the wake shed by the rotor hub could result in a strong blade wake interaction noise. As a VAWT rotates, the lift, and therefore the circulation, on the blades fluctuates, meaning that they will shed vorticity. At lower tip speed ratios, the blades may also experience dynamic stall, during which strong vortices are shed. The downstream blades will interact with the vertical wake from the upstream blades and this may generate impulsive blade loads by blade-vortex interaction. As the blade passes a vortex generated by a previous blade passage it experiences a change in angle of attack due to the vertical velocity component induced by the vortex. This in turn causes a change in lift on the blade and hence according to acoustic analogies produces a dipole type tonal noise.

2.3 Incoming turbulence noise

The loads on an aerofoil are strongly dependent on the flow conditions. If the oncoming flow is turbulent this will generate fluctuating loads on the blades, which will result in noise being radiated (see Amiet [1975]). As with the aerofoil self-noise, the radiated sound is highly dependent on the exact nature of the turbulent inflow. Unfortunately, it is very challenging to accurately characterise the turbulence in the wind, since it is governed by a wide range of parameters such as the surface roughness and the atmospheric temperature gradient. Detailed descriptions of some of the relationships that govern the levels of large-scale atmospheric turbulence are presented in the thesis by McIntosh [2009]. There is very little published information about the small scales of atmospheric turbulence and this is for two reasons.

Firstly, the vast majority of the energy in the wind is contained in the larger structures, commonly known as gusts, so from the perspective of power generation the small scales are irrelevant. Secondly, the local surface roughness will affect the turbulence spectra [McIntosh, 2009], meaning the small scales are likely to be strongly site specific. A scaling relationship for turbulent inflow noise was derived by Amiet [1975] and subsequently adapted by Glegg et al. [1986] for use in wind turbine noise simulations.

2.4 Other sources of aeroacoustic noise

Aerofoil self-noise is the noise generated by the interaction between an aerofoil and the flow disturbances produced in its own boundary layer and near wake. Brooks, Pope, and Marcolini [1989] wrote the definitive work on empirical self-noise modelling where they grouped these interactions into five categories and developed correlations for predicting the sound radiated by each source. The five source terms are:

1. Turbulent boundary layer trailing edge noise.
2. Separation/stall noise.
3. Laminar boundary layer vortex shedding noise.
4. Trailing edge bluntness vortex shedding noise.
5. Tip vortex formation noise.

The relative magnitude of these sources is dependent on the exact flow conditions over the aerofoil. In many practical applications, where the boundary layer is turbulent, the laminar boundary layer vortex shedding noise can be ignored since it is much quieter than the turbulent trailing edge noise. Fink and Bailey [1980] also noted that during stall the noise level can be up to 10dB greater than the noise due to TBL-TE noise at low angles of attack. At moderate angles of attack, the noise was still found to be due to the passage of turbulent, separated flow over the trailing edge, while at higher angles of attack the noise was radiated from the chord as a whole [Paterson et al., 1973].

3. Dynamics of VAWT

The aerodynamics of a lift-type VAWT are fundamentally unsteady. As the blade rotates around the hub the angle between the blade velocity and the wind velocity varies significantly. This creates a variation in angle of attack and hence a variation in the aerodynamic forces exerted on the blades. The magnitude of this variation is governed by the tip speed ratio (TSR) which is defined as the ratio of the blade speed to the wind speed. An approximation of the variation in blade angle of attack can be calculated using simple geometry by assuming that the free stream flow is uniform in both magnitude and direction over the whole rotor. This ‘geometric’ variation in angle of attack is shown in figure 2 for a range of TSR. It is important to note that the geometric angle of attack varies from the true angle of attack due to the deflection of the incoming flow by the rotor.

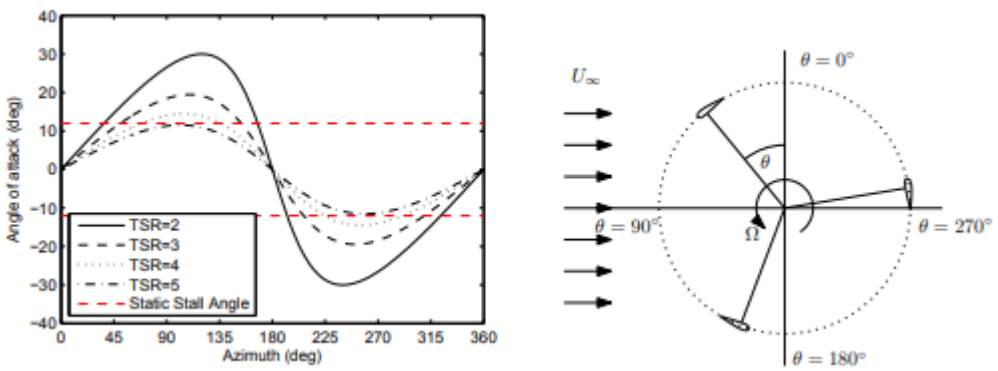

Fig 2. - VAWT blade angle of attack during one rotation at different TSR

From figure 2 it is clear that at low TSR the blades pass the static stall angle as they approach the most upstream point of the rotation. Since the angle of attack is constantly changing, the blades will experience dynamic stall at low TSR. As the TSR increases, the extent of the stall in the upstream half of the rotor decreases, which increases the amount of torque that the blades generate since the lift to drag ratio remains higher. The higher blade speed however, increases the level of parasitic drag on the rotor which simultaneously reduces the torque generated by the rotor. As such the design of a VAWT rotor is a trade-off between minimising both stall and drag in order to achieve maximum performance (figure 3).

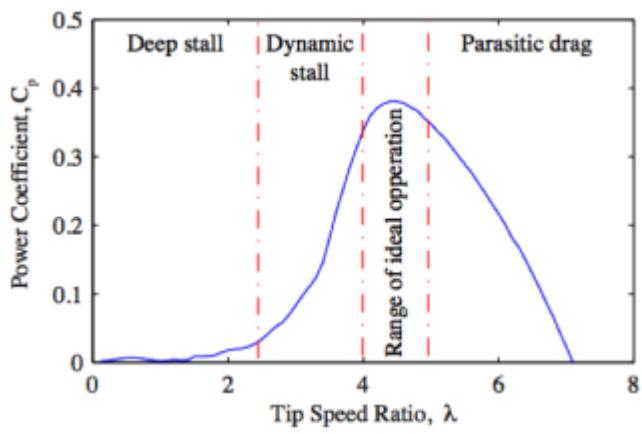

Fig 3. - Power coefficient optimisation vs TSR

The second key feature of VAWT operation is the fact that the blades in the upstream half of the rotation shed a wake that passes through the rotor and interacts with the blades in the downstream half of the rotation. This effect is exaggerated by the influence of the tip vortices shed by the upstream blades since their direction of rotation tends to cause the wake at the top and bottom of the rotor to be deflected towards the mid-span of the downstream blades.

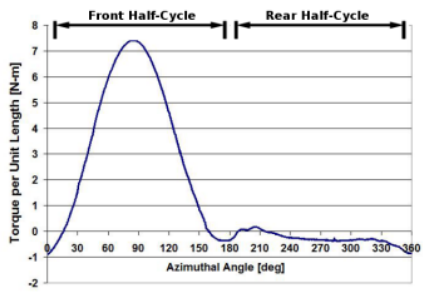

Fig 4. - Typical torque for one blade during complete rotation

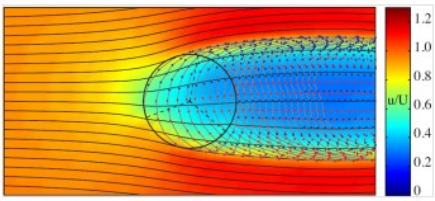

Fig. 5 - Velocity field after flow passing the VAWT

This potentially introduces further unsteady blade loading that could affect the noise radiated by a VAWT rotor. A typical torque graph produced by one blade during a full 360 ^{0} cycle is presented in figure 4.
It can be seen that most of the power is produced within from half cycle where the kinetic energy extraction is maximum. The remaining flow has a smaller average velocity due to this blockage effect as can be seen in figure 5.

4. Aerodynamic noise mitigation and performance enhancement using Coflow-jet principle

CFJ method consists in adding injection slots near the leading edge and suction slots near the trailing edge of a basic airfoil, as in figure 6. Air is injected near the LE and extracted near the TE using a recirculation pump, so we have the case of zero net mass flux since the mass of injected air is equal with the extracted mass.

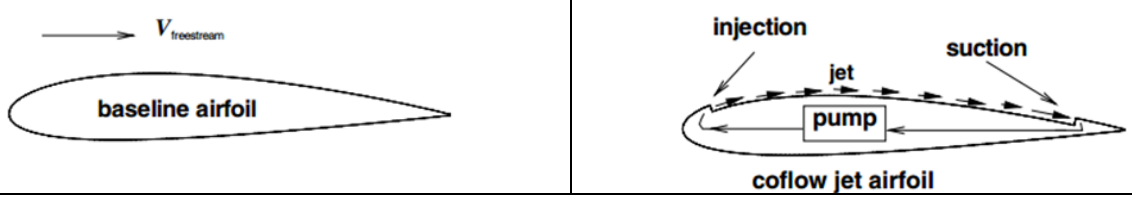

Fig. 6 - Coflow jet (CFJ) principle

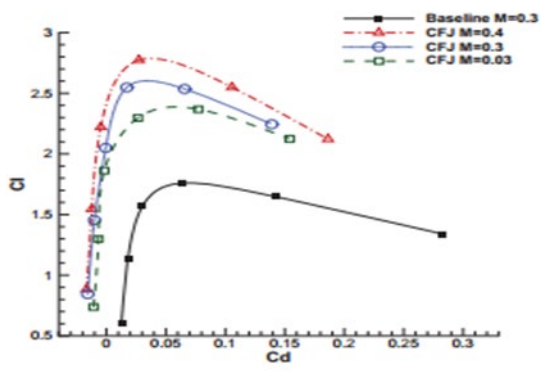

Fig.7 - Aerodynamic characteristics for base and CFJ airfoils

The aerodynamic results of such circulation are: increased boundary limit momentum, much higher stall AoA, decreased wake, much higher lift and a reduced induced drag. It must be mentioned that for some configurations it is possible to achieve even a negative induced drag which makes the solution highly attractive for new airplanes design. A typical performance graph showing Lift and Drag coefficients of CJF and baseline airfoils are presented in figure 7.

From an aeroacoustic point of view, the delayed stall produces less wake behind the profiles so it was expected that in case of VAWT to find a decrease of the blade-wake interaction noise.

5. CFD and Aeroacoustic simulation

5.1 Geometry and mesh

Numerical 2 D study was conducted on 3 blades, H-type VAWT with the following characteristics: R= 1.2 m; Basic blade profile NACA0021 with C=0.3 m. For CJF modified profile we used: $h_{injection\ slot}$ = 0.002 m; $h_{succion\ slot}$ =0.004 m. Injection and suction slots are placed at 6% chord and 80% chord distance from the leading edge as can be seen in figure 8.

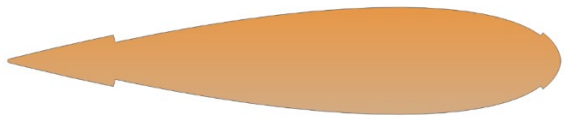

Fig. 8 - CFJ airfoil for VAWT

Injection and suction slots were used on both sides of the airfoils due to the fact that during a complete rotation the angle of attack oscillates between negative and positive values so the suction side becomes pressure side. It should be mentioned that it is possible to use active control of the jets in order to use them alternatively only for the suction side.

The domain was divided in 3 circular parts, two static and one rotating containing the turbine blades (as seen in figure 9). Mesh was structured for the static domains and partially structured for the rotating domain. We used a number of 845000 cells and 853000 nodes. For the boundary layer we used an y^+ = max. 2.2 which was calculated after the simulation. Total domain D1 diameter was 6 times the VAWT diameter in order to keep the acoustic sources information inside.

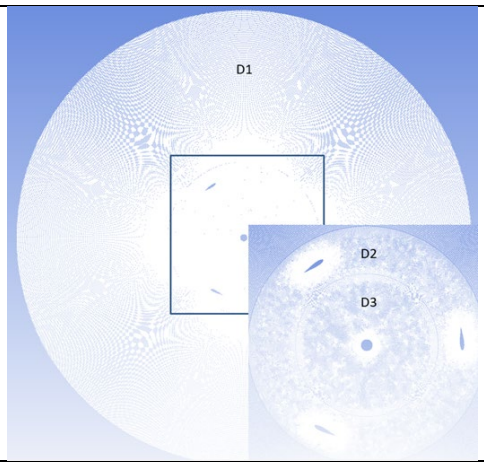

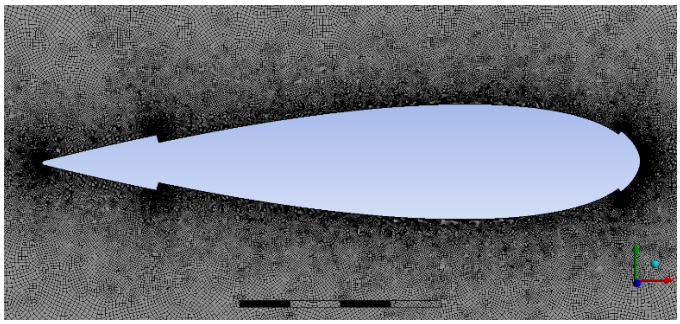

Fig. 9 - Domains and mesh

5.2 Numerical simulation

Numerical algorithm

Numerical simulation for aerodynamic and acoustic field was conducted with Ansys Fluent software. For the aerodynamic analysis, we used URANS and SST turbulence model. Transitory analysis was made using an implicit scheme using a time step which correspond to 1 degree of rotation. Every time step was iterated by 20 times. In the current paper, the discretization algorithm was conducted by SIMPLE with second-order upwind scheme by under-relaxation factors for ensuring convergence of iterative computations. The transient formulation was performed by second order implicit. Simulations were performed for Basic and CFJ airfoils at TSR 1.5; 2; 2.5. Injection and suction mass flow were established for each TSR in order to have no stall at maximum angle of attack for that configuration. This resulted from separated steady flow RANS simulations using CFJ airfoils at different attack angles and flow speed. This resulted in the minimum injection mass flow which was later used as a boundary condition for the VAWT simulation.

Boundary conditions

Parameter	Value
Incoming far field velocity	10 m/s
Turbulent intensity far-field	5%
Flow density	1.225 kg/m^3
Dynamic viscosity 1.789x10^{-5}	1.789 x 10^{-5} Ns/m^2
Turbulent intensity injection –suction slots	5%
Injection speed	90 m/s
Suction speed	45 m/s
Walls	Non-slip condition

6. Results

Aerodynamic and acoustic results show some interesting information by using the Coflow jet for a VAWT. Even that the main purpose of this study was the acoustic field evaluation, aerodynamic performance as Momentum coefficient are presented.

6.1 Aerodynamic performance

The use of CFJ for the VAWT increases the output power by reducing or completely eliminating the stall of the airfoils and due to the reactive force which appears due to the jets. However, this performance comes to a cost, which is the power consumption of the jets which must be evaluated and subtract it from the overall generated power by the VAWT. Since the study was dedicated to the acoustic field, this evaluation was not conducted here. Data and results regarding the Momentum coefficient (CM) and the comparison between Baseline (no jet) and CFJ solution for TSR 1.5; 2; 2.5 are presented below.

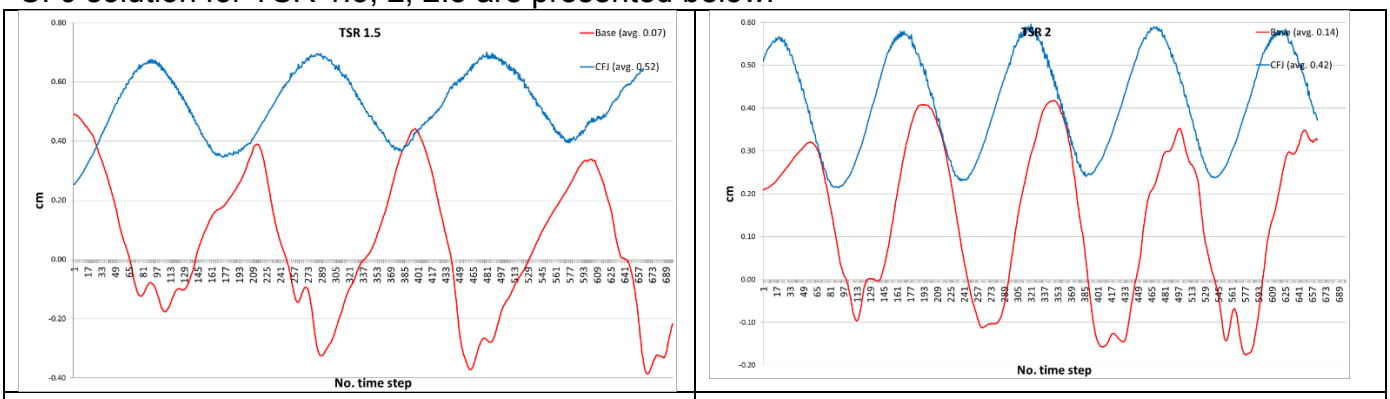

a) b)

Fig. 10 - Momentum coefficient (cm) Base vs CFJ a) TSR1.5; b) TSR2; c) TSR 2.5.

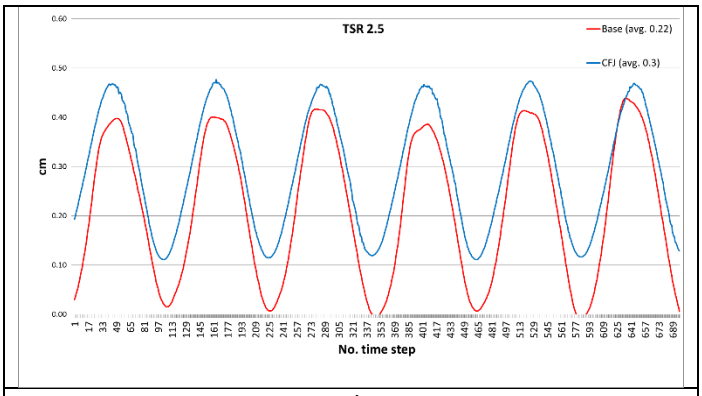

c)

Aerodynamic performance is dramatically improved by CFJ solution especially for low TSR.
It is worth to mention that this performance is achieved by using a supplementary power to inject the air. However, it has been previously demonstrated that it is possible to achieve a net gain using the CFJ as a super circulation method.

6.2 Aeroacoustic performance

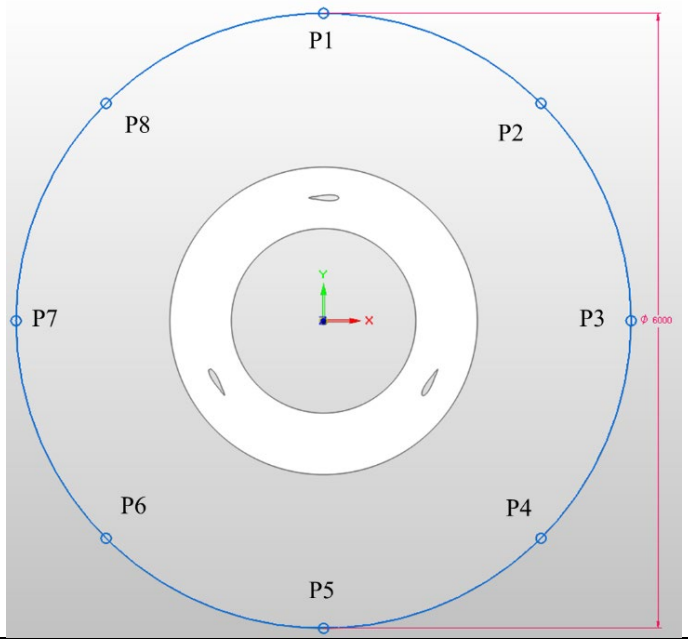

Fig. 11 - Receivers distribution

The acoustic field around the wind was calculated using the Ffowcs Williams-Hawkings analogy. We distributed 8 receivers around the turbine at 3 m distance from the rotating axis as can be seen from figure 11.
OASPL values for each receiver were calculated for TSR 1.5 ;2; 2.5 and are presented within Table 1. The values were calculated for overall frequency domain (0-600 Hz), infrasound (0-20Hz) and sound (20- 600 Hz) comparing Base with CFJ solution.

Table1 - OASPL for different receivers

Case	Virtual mic	Frequency domain dB					
		0-600Hz		0-20Hz		20-600Hz	
		Base	CFJ	Base	CFJ	Base	CFJ
TSR1.5	P1	99.4	97.9	99.2	97.8	85.7	82.6
	P2	96.6	95.7	96.2	95.4	85.2	82.9
	P3	100.4	99.2	100.1	99.0	87.2	85.6
	P4	104.7	103.2	104.5	103.1	90.4	86.7
	P5	106.9	106.0	106.8	105.9	87.9	86.4
	P6	106.3	105.4	106.3	105.3	86.4	85.9
	P7	106.7	106.1	106.6	106.0	91.4	89.5
	P8	105.0	104.6	104.8	104.4	90.4	89.5
	Lp_avg	**104.5**	**102.7**	**104.3**	**102.6**	**88.6**	**86.3**
	Diff.	**-**	**1.8**	**-**	**1.8**	**-**	**2.3**
TSR2	P1	98.6	97.0	98.4	96.8	85.91	82.70

	P2	96.2	93.7	95.9	93.5	84.38	79.91
	P3	98.7	98.0	98.4	97.9	87.02	83.59
	P4	103.9	102.3	103.7	102.2	89.68	84.26
	P5	106.8	105.0	106.7	104.9	90.08	84.65
	P6	107.5	106.5	107.5	106.5	85.44	83.97
	P7	107.7	106.4	107.6	106.4	89.30	84.75
	P8	105.0	104.1	104.9	104.0	90.48	88.45
	Lp_avg	**104.7**	**103.4**	**104.6**	**103.4**	**88.3**	**84.6**
	Diff.	**-**	**1.3**	**-**	**1.3**	**-**	**3.7**
TSR2.5	P1	102.1	93.9	101.5	93.8	93.11	77.20
	P2	97.9	88.4	97.6	88.2	86.88	74.96
	P3	98.6	93.1	98.4	93.0	85.64	77.81
	P4	102.1	96.9	101.9	96.8	89.46	81.82
	P5	105.2	99.6	104.9	99.6	93.22	79.55
	P6	107.5	102.1	107.4	102.0	88.43	82.75
	P7	107.9	102.8	107.9	102.7	87.62	85.20
	P8	106.5	100.8	106.4	100.8	90.06	81.46
	Lp_avg	**104.8**	**99.2**	**104.7**	**99.1**	**90.1**	**81.2**
	Diff.	**-**	**5.6**	**-**	**5.5**	**-**	**8.9**

It can be seen that it is possible to achieve an important noise reduction on all frequencies and even more on audible domain. The max average reduction of 8.9 dB was obtained for TSR 2.5 case. The explanation might be that for this TSR the jets speed was optimised in order to be the minimum speed at which stall is not present.

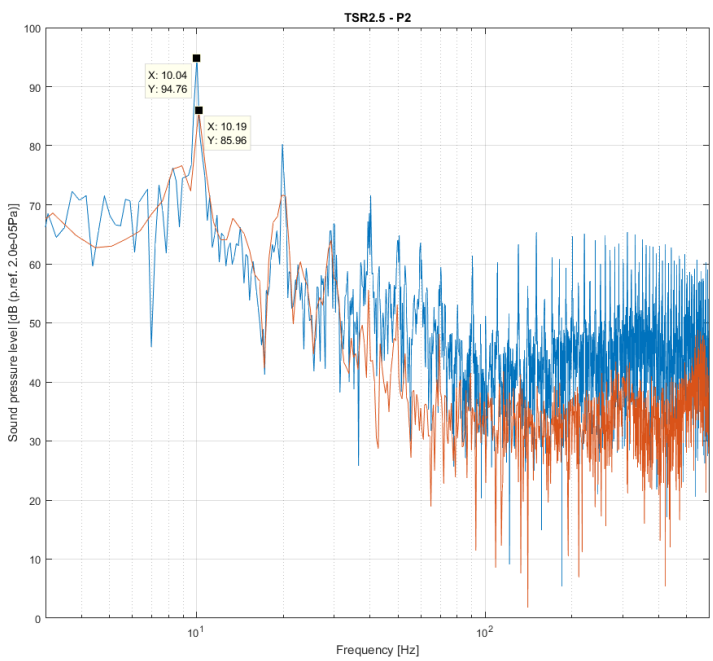

Fig. 12 - Noise spectrum analysis (Base - blue; CFJ - orange)

For smaller TSR it is possible that the jets were to strong and can add some broadband jet noise.
An interesting finding is that CFJ is capable to strongly reduce the tonal noise as can be seen from the FFT analysis at receiver P2 and presented in figure 12.
This was an expected result since the wake reduction due to CFJ reduces also the blade-wake interaction which is the main tonal noise source.
Another interesting finding is that VAWT noise has a distinct directivity and can be altered by the use of CFJ as can be seen from the figure 13.

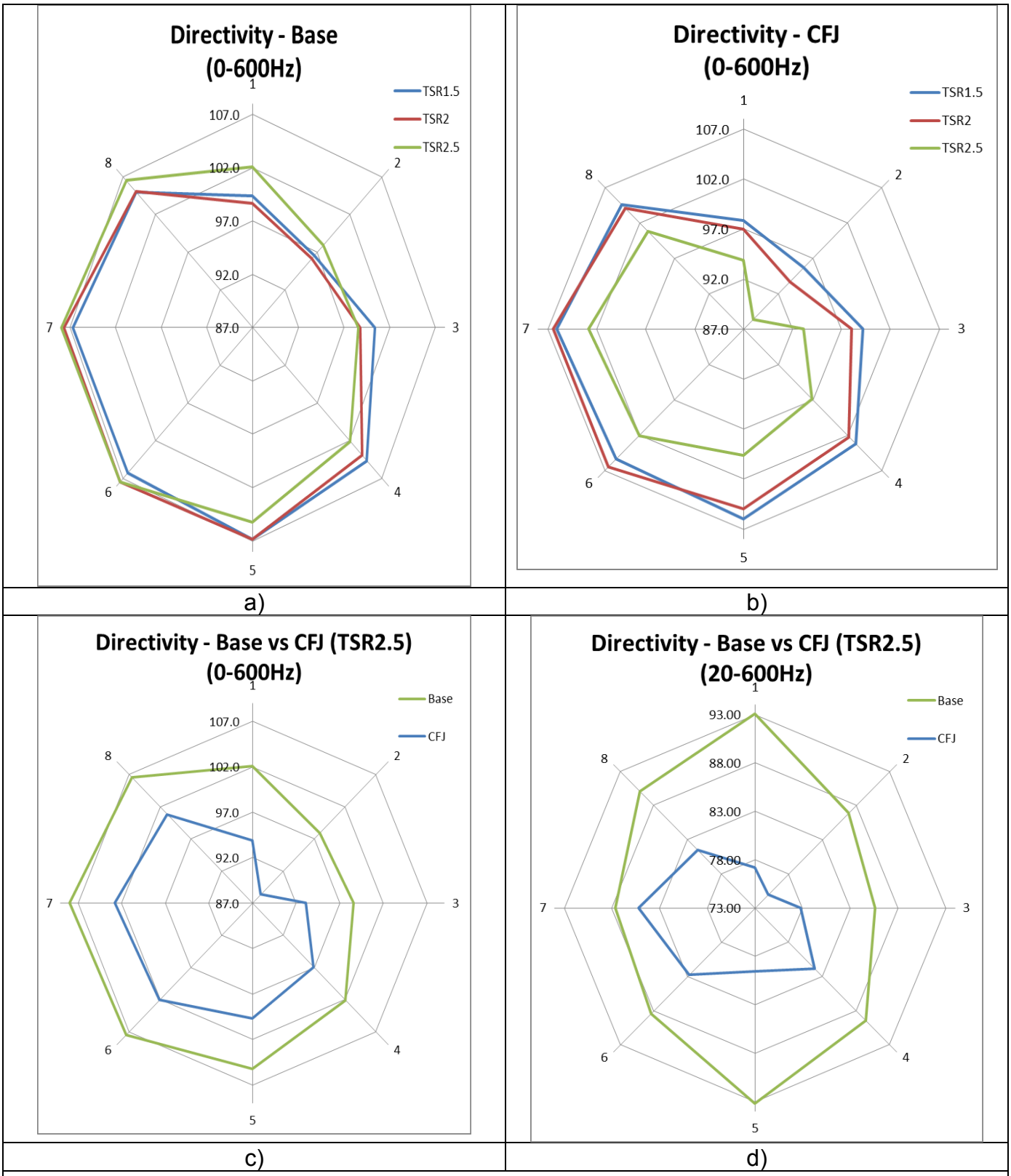

Fig. 13 - a) noise directivity base b) directivity CFJ c) directivity base vs CFJ TSR2.5 d) directivity base vs CFJ TSR 2.5 (20-600Hz)

It can be seen that CFJ can also modify VAWT noise directivity as can be seen in figure 13 d).

7. Conclusions

CFJ VAWT represents an interesting option for wind energy harvesting since it is efficient and quieter. Efficiency is much higher than the base but requires additional input power to recirculate the jet. However, it has been demonstrated by other authors that it is possible to achieve an important net gain in power output. Several interesting findings about noise field

have been revealed by this study. The most important is that it is possible to get a strong OASPL reduction both broadband and tonal. This is the effect of wake reduction and thus the blade-noise interaction. These findings require a future investigation for the possibility of optimization the CFJ VAWT in terms of efficiency and noise production.

References

Paraschivoiu I.,Saeed F., Desobry V.(2002) *"Prediction capabilities in vertical axis wind turbine aerodynamics"* Berlin, Germany

Castelli M.R.(2012) *„Effect of blade number on a straight – bladed vertical axis Darrieus wind turbine"*, World Academy of Science, 61

Ferreira S., Bijl H., G. Van Bussel,G van Kuik(2007) *„Simulating dynamic stall in a 2D VAWT"*, Journal of Physics, Conference Series 75

RK Amiet (1976) "*Noise due to turbulent flow past a trailing edge*" Journal of Sound and Vibration, 47(3):387{393}. 16, 79

T Brooks (1993) *"Studies of blade-vortex interaction noise reduction by rotor blade Modification"* NASA STI/Recon Technical Report A, 959:90093. ix, 29

M Castelli, A Villa, and E Bernini (2011) "*CFD Analysis of the Influence of Central Shaft on Vertical Axis Wind Turbine Noise Emission"* In International Wind Turbine Noise Conference, Rome. x, 52, 56

C Ferreira (2009) "*The near wake of the VAWT: 2D and 3D views of the VAWT aerodynamics*" PhD thesis, Technische Universiteit Delft, . 6, 36, 40, 51, 53

S McIntosh (2009) *"Wind Energy for the Built Environment"* PhD thesis, University of Cambridge. x, xiii, 3, 20, 21, 36, 38, 39, 42, 45, 46, 49, 53, 88, 142, 144, 152

Zha, G.-C. and Paxton C. (2004) *"A Novel Airfoil Circulation Augment Flow Control Method Using Co-Flow Jet"* AIAA Paper 2004-2208, 2nd AIAA Flow Control Conference, Portland, Oregon.